Theory of tapered cooling

Hiromi Okamoto
Accelerator Laboratory, Institute for Chemical Research, Kyoto University, Gokanoshou, Uji, Kyoto 611, Japan

Jie Wei
Brookhaven National Laboratory, Upton, New York 11973

(Received 26 March 1998)

A theory of tapered cooling for fast circulating ion beams in a storage ring is constructed. We describe the fundamentals of this cooling scheme, a scheme that effectively yields both transverse and longitudinal cooling through radial-position-dependent longitudinal momentum cooling, emphasizing that it might be the most promising way to beam crystallization. The cooling rates are analytically evaluated to study the ideal operating condition. We discuss the physical implication of the tapering factor of the cooling force, and show how to determine its optimum value. Molecular dynamics is employed to demonstrate the validity of the present theory. [S1063-651X(98)13009-X]

PACS number(s): 41.75.−i, 52.60.+h, 29.20.Dh, 61.50.−f

I. INTRODUCTION

The phase transition of fast ion beams in a storage ring has attracted a great deal of interest since Russian physicists reported on a sudden jump of the Schottky signal detected in the NAP-M ring [1]. Discussions held on the interpretation of the NAP-M results eventually initiated the comprehensive study of the ultracold state of particle beams. These beams are sufficiently cold in the beam rest frame, so that particles making up the beam ''lock into'' a position where the repelling Coulomb force just balances the external focusing force. Seen in the laboratory frame, the whole ordered structure circulates at great speed. The concept of the crystalline beam, regarded as a new state of matter, has now opened up various future possibilities in fundamental and applied physics areas, including the study of completely space-charge-dominated beams, the study of Wigner crystal, the realization of high-luminosity ion colliders, the application to ultrahigh resolution nuclear experiments and to atomic physics research, etc.

The subject of beam crystallization was first studied using the molecular dynamics (MD) approach by Schiffer and coworkers [2]. In recent years, Wei, Li, and Sessler demonstrated theoretically that beam crystallization is practically achievable in a properly designed storage ring with a sufficiently strong three-dimensional (3D) cooling force [3]. However, in order to reach a crystalline ground state, we still need to develop cooling methods that are much more powerful than what has been conventionally used.

Laser cooling [4], whose limiting temperature is of the order of mK, is so far the most promising method to attain crystalline beams. During recent years, extensive experimental efforts have been made to achieve a longitudinal beam temperature in the mK range [5,6]. However, since laser cooling works on the Doppler principle, it does not produce direct transverse cooling. Although intrabeam Coulomb scattering exchanges heat between transverse and longitudinal directions, and the corresponding sympathetic cooling has been reported [7], the cooling process is too slow. The transverse beam temperatures achieved in past experiments are simply too high for our final goal.

To overcome this difficulty, several methods applying artificial dynamical coupling have been proposed. The simplest 3D laser cooling scheme is to use momentum dispersion at a regular rf cavity installed on a ring [8]. It has been shown both analytically and numerically that one can enhance the transverse cooling rates up to the same level as the longitudinal rate. Introduction of a coupling cavity operating in the TM_{210} mode is an alternative, mathematically equivalent scheme [9]. We have verified that the coupling cavity improves the transverse cooling efficiency even more. According to the latest MD study [10], the equilibrium transverse temperature achievable with these methods appears to be in the region of 0.01 K or less, far below the current achievable range. In fact, we have successfully observed Coulomb ordering in numerical simulations where only realistic longitudinal cooling devices are used. But, unfortunately, these schemes are limited to azimuthally bunched beams. Furthermore, in order to make the coupling effective, the machine must operate near a linear synchrobetatron resonance in every lattice period, which usually conflicts with the requirement for crystal maintenance [11]. In the above-mentioned MD simulations, the maintenance condition was actually broken since we considered only a single rf cavity (and a single coupling cavity) in a ring. Consequently, the ordered structures would quickly melt away once the cooling force was removed.

The concept of tapered cooling was first introduced as a possible way to achieve a final crystalline state where momentum $(\delta p/p)$ is a function of the radial displacement (x) [12,13]. Recently, systematic studies [14] concluded that tapered cooling not only works at low temperature, but works at any finite temperature by effectively cooling both transverse (betatron) and longitudinal phase space. In this scheme, particles at different radial positions are cooled towards different momenta. The change in momentum deviation at the cooling device is expressed in the laboratory frame by

$$\Delta\left(\frac{\delta p}{p}\right) = -f_s\left[\left(\frac{\delta p}{p}\right) - \gamma C_{\mathrm{xs}}\frac{x}{\rho_m}\right], \tag{1}$$

where ρ_m is the average radius of curvature in the bending sections of the storage ring, $\gamma=1/\sqrt{1-\beta^2}$ is the Lorentz factor, f_s is a positive constant corresponding to the cooling strength, and we call $C_{\rm xs}$ the *tapering factor* [15]. While the tapered force does not directly affect the vertical motion, the dissipative effect can readily be extended to this direction by introducing a linear coupling between the horizontal and vertical degrees of freedom [8,9], which is easily done by means of a skew quadrupole magnet in a ring.

Experimentally, we can realize tapered laser cooling by employing a special light whose photon frequency has a linear dependence on the horizontal coordinate. Such a laser could be obtained, for example, by means of a prism. Similarly, we can generate the tapered electron cooling force by utilizing the dispersive effect from a bending magnet [16]. As demonstrated below, the tapered cooling scheme enables one to reach all kinds of crystalline structure if the ring lattice satisfies the necessary conditions [11].

In this paper, we give a theoretical description of the physics of tapered cooling. First, we review the Hamiltonian formalism for the study of space-charge-dominated beams in Sec. II. In Sec. III, the cooling rates are evaluated under the linear approximation, and the stability limit of a laser-cooled beam is discussed. We then show, in Sec. IV, how to optimize the tapering factor to crystallize fast circulating beams. Finally, in Sec. V, the theoretical predictions are compared with MD simulation results.

II. MEAN-FIELD HAMILTONIAN FORMALISM

Before proceeding to the details of the tapered cooling scheme, we first briefly outline a Hamiltonian formalism for the study of cold beams. A general theory of space-charge-dominated beams is available in Ref. [17].

The starting point is the variational principle

$$\delta\int L_t dt=0, \tag{2}$$

where L_t is the relativistic Lagrangian describing the motion of a charged-particle beam. For later convenience, we change the independent variable from the time t to the reference path length s, modifying Eq. (2) to $\delta\int L_s ds=0$ in terms of the new Lagrangian

$$L_s=-mc\sqrt{(ct')^2-\mathbf{u}'\cdot\mathbf{u}'}+q(\mathbf{A}\cdot\mathbf{u}'-\phi t'), \tag{3}$$

where q and m are, respectively, the charge state and rest mass of stored ions, c is the speed of light, $\mathbf{u}$ is the coordinate vector in real space, ϕ is the scalar potential of space charges satisfying Poisson's equation, $\mathbf{A}=(A_x,A_y,A_s)$ includes the potential of the space-charge field as well as that of external magnetic fields, and the prime stands for differentiation with respect to s. Without loss of generality, we consider only coasting beams for simplicity [18] and thus neglect the longitudinal component of space-charge force (i.e., $A_x=0=A_y$). The Hamiltonian can now be derived, from L_s, as

$$H=-\left(1+\frac{x}{\rho}\right)\sqrt{\left(\frac{p_t+q\phi}{c}\right)^2-m^2c^2-p_x^2-p_y^2}-q\left(1+\frac{x}{\rho}\right)A_s, \tag{4}$$

where ρ is the curvature of the reference orbit and the longitudinal canonical momentum conjugate to t has been introduced as $p_t=\partial L_s/\partial t'$. Expanding the square root and keeping the low order terms, we obtain

$$H\approx-\left(1+\frac{x}{\rho}\right)\left(qA_s+p-\frac{p_x^2+p_y^2}{2p}\right), \tag{5}$$

where p is the total kinetic momentum given by $p=m\beta\gamma c=\sqrt{(p_t+q\phi)^2/c^2-m^2c^2}$. Taking only bending and quadrupole magnets into account [19], Eq. (5) becomes

$$H\approx-p_0\left(1+\frac{x}{\rho}\right)\frac{\Delta E}{\beta_0^2E_0}+\frac{p_0}{2\gamma_0^2}\left(\frac{\Delta E}{\beta_0^2E_0}\right)^2+\frac{p_x^2+p_y^2}{2p_0}+\frac{p_0}{2}(K_xx^2+K_yy^2)+\frac{q}{\beta_0c\gamma_0^2}\phi, \tag{6}$$

where the quantities with the subscript 0 express the values of the reference particle, K_x and K_y are the horizontal and vertical focusing functions respectively, and $\Delta E=E-E_0$ is the total energy difference from the design value E_0. Using the Suzuki's generating function [20] and then adopting the relative time $\tilde{t}=t-s/\beta_0c$ as the longitudinal coordinate, H is transformed to

$$\tilde{H}=\frac{1}{2}(\tilde{p}_x^2+K_x\tilde{x}^2)+\frac{1}{2}(\tilde{p}_y^2+K_y\tilde{y}^2)+\frac{1}{2}\left[\frac{1}{\gamma_0^2}+D_x\left(\frac{q}{p_0\beta_0c\gamma_0^2}F_{\rm sc}-\frac{1}{\rho}\right)\right]\left(\frac{\Delta\tilde{E}}{\beta_0c}\right)^2+\frac{q}{p_0\beta_0c\gamma_0^2}\left(\tilde{\phi}-F_{\rm sc}\tilde{x}\frac{\Delta\tilde{E}}{\beta_0c}\right), \tag{7}$$

where the new canonical variables of the system are $(\tilde{x},\tilde{p}_x,\tilde{y},\tilde{p}_y,\tilde{t},\Delta\tilde{E})$, the function $\tilde{\phi}$ is related to the original Coulomb potential as $\tilde{\phi}=\phi(x=\tilde{x}-D_x\Delta\tilde{E}/\beta_0c,y=\tilde{y};s)$, and $F_{\rm sc}$ is the s-dependent periodic function associated with the space-charge detuning to the horizontal dispersion function D_x [21]; namely,

$$D_x''+K_xD_x=\frac{1}{\rho}+\frac{q}{p_0\beta_0c\gamma_0^2}F_{\rm sc}. \tag{8}$$

It is evident from Eq. (7) that the longitudinal canonical momentum is a constant of motion. We therefore write $\Delta\tilde{E}\equiv W=$ const. In this case $F_{\rm sc}$ may generally involve W as a parameter. The horizontal betatron equation derived from $\tilde{H}$ suggests that it is beneficial to define $F_{\rm sc}$ as

$$\frac{W}{\beta_0c}F_{\rm sc}=\left(\frac{\partial\tilde{\phi}}{\partial\tilde{x}}\right)_{\tilde{x}=0=\tilde{y}}, \tag{9}$$

such that the linear force terms balance along closed orbits in a ground state. For crystalline beams under a mean-field approximation, F_{sc} is proportional to D_x and independent of W as shown later, due to the linearity of the potential ϕ [see Eq. (22)].

III. COOLING RATES

In this section, we demonstrate that tapered cooling effectively reduces the temperature in both transverse and longitudinal directions. Cooling rates, operating points, and stability limits are discussed at high temperature, neglecting intraparticle interaction.

A. Evaluation of the linear cooling rates

In the high temperature regime, we can simplify the Hamiltonian of Eq. (7) by neglecting the space-charge potential. It is then possible to express the solution of the equations of motion by a transfer matrix $\mathbf{M}(s_1|s_0)$ for the canonical variables from position s_0 to s_1, which are defined by

$$(\tilde{x},\tilde{p}_x,\tilde{y},\tilde{p}_y,\tilde{t},\Delta\tilde{E})(s_1)=\mathbf{M}(s_1|s_0)(\tilde{x},\tilde{p}_x,\tilde{y},\tilde{p}_y,\tilde{t},\Delta\tilde{E})(s_0).$$

For the section of the machine consisting of regular bending dipoles and alternating-gradient (AG) focusing quadrupoles, the transfer matrix from the Hamiltonian $\tilde{H}$ is written as [22]

$$\mathbf{M}_D=\begin{pmatrix} \cos\mu_x & \frac{R\sin\mu_x}{\nu_x} & \mathbf{0} & \mathbf{0} \\ -\frac{\nu_x\sin\mu_x}{R} & \cos\mu_x & & \\ \mathbf{0} & & \cos\mu_y & \frac{R\sin\mu_y}{\nu_y} \\ & & -\frac{\nu_y\sin\mu_y}{R} & \cos\mu_y \end{pmatrix}, \tag{10}$$

where the horizontal and vertical betatron tunes are denoted by ν_x and ν_y, respectively, η is the phase slip factor, R is the average ring radius, $\mathbf{0}$ represents the 2×2 zero matrix, $\mu_x=2\pi\nu_x$, and $\mu_y=2\pi\nu_y$. The effect of tapered cooling can be expressed by a second transfer matrix just across the cooling device, obtained by linearizing Eq. (1),

$$\mathbf{M}_{TC}=\begin{pmatrix} 1-g & 0 & \mathbf{0} & 0 & (g-f_s)\frac{d_c}{\beta_0 c} \\ 0 & 1 & & 0 & 0 \\ \mathbf{0} & & \begin{matrix}1&0\\0&1\end{matrix} & & \mathbf{0} \\ 0 & 0 & & 1 & 0 \\ -\frac{g\beta_0 c}{d_c} & 0 & \mathbf{0} & 0 & 1-f_s+g \end{pmatrix}, \tag{11}$$

where d_c is the magnitude of momentum dispersion in the cooling section, and g is the dimensionless parameter defined by $g\equiv\gamma_0 f_s C_{xs} d_c/\rho_m$. Specifically, d_c must be finite to produce a horizontal dissipative force. The effect of the skew quadrupole magnet, needed to couple transverse motion for a simultaneous cooling in both horizontal and vertical directions, is

$$\mathbf{M}_Q=\begin{pmatrix} & & 0 & 0 & & \\ \mathbf{I} & & -\frac{\Gamma_q}{R} & 0 & \mathbf{0} & \\ 0 & 0 & & & 0 & 0 \\ -\frac{\Gamma_q}{R} & 0 & \mathbf{I} & & 0 & \frac{d_q\Gamma_q}{R\beta_0 c} \\ & & -\frac{d_q\Gamma_q}{R\beta_0 c} & 0 & & \\ \mathbf{0} & & & & \mathbf{I} & \\ & & 0 & 0 & & \end{pmatrix}, \tag{12}$$

where d_q is the dispersion size at the skew magnet, $\mathbf{I}$ denotes the identity matrix, and Γ_q is the coupling constant. For a quadrupole magnet having the axial length ℓ_q, Γ_q is defined by $\Gamma_q/R=\ell_q/B\rho\,\partial B/\partial y$, where B is the magnetic field.

The linear cooling rates in the transverse and longitudinal directions are defined as the reduction per unit s of the relative transverse oscillation amplitude and momentum W. It can be obtained by evaluating the eigenvalues of the one-tune transfer matrix $\mathbf{M}=\mathbf{M}_D\cdot\mathbf{M}_Q\cdot\mathbf{M}_{TC}$. Substituting Eqs.

TABLE I. TARN II machine and beam parameter used for simulation.

Quantity	Value
Ring circumference	77.7 m
Horizontal tune ν_x	1.68–2.1
Vertical tune ν_y	1.7–2.3
Transition energy	1.82–2.29
Skew quad integral strength per lattice period	0.02 m^{-1}
Dipole bending radius ρ_m	4.01 m
Ion species	$^{24}Mg^+$
Kinetic energy	1 MeV
Relativistic factor γ	1.000 044
Dispersion at cooling station d_c	3.4–5.0 m
Dispersion at skew quad d_q	1.7–2.9 m

(10), (11), and (12) into the characteristic equation $|\mathbf{M}-\lambda\mathbf{I}|=0$, we eventually find the dispersion relation

$$\left(\lambda+\frac{1}{\lambda}-2\cos\mu_y\right)\times\left\{(\lambda-1+f_s-g)\left[\lambda+\frac{1-g}{\lambda}-(2-g)\cos\mu_x\right]-g(g-f_s)\left(\frac{1}{\lambda}-\cos\mu_x\right)\right\}-\Gamma\left\{\left[1-\left(1-\frac{d_q}{d_c}\right)g\right]\lambda-1+f_s\right\}=0, \tag{13}$$

where $\Gamma\equiv(2\pi\Gamma_q)^2\sin\mu_x\sin\mu_y/\mu_x\mu_y$. When writing $\lambda=\exp(i\mu)$, the imaginary part of μ can be directly related to the cooling rates. A larger $\mathrm{Im}(\mu)$ implies a higher cooling rate while the beam becomes unstable if $\mathrm{Im}(\mu)<0$.

As an example, we choose among a wide range of choices, the beam and machine parameters of the storage cooler ring TARN II listed in Table I [23]. In Fig. 1 we display numerical solutions of Eq. (13) under a strong cooling situation. We recognize that one of the three cooling rates becomes negative beyond a certain C_{xs}; in other words, too steep tapering causes beam heating. It can be shown that there always exists a threshold value of C_{xs} beyond which the cooling process becomes unstable.

B. Operating point consideration and limiting tapering factor

For a more practically achievable cooling rate of $f_s\ll 1$, we can solve Eq. (13) analytically to discover scaling laws for the cooling rates and stability limits. When horizontal and vertical tunes are well separated, the cooling rates can be obtained by using the perturbative method,

$$\begin{aligned}&\mathrm{Im}(\mu)\approx 2GC_{\mathrm{xs}} && \text{(for the horizontal motion)}\\ &\mathrm{Im}(\mu)\ll f_s && \text{(for the vertical motion)}\\ &\mathrm{Im}(\mu)\approx f_s-4GC_{\mathrm{xs}} && \text{(for the longitudinal motion)}\end{aligned} \tag{14}$$

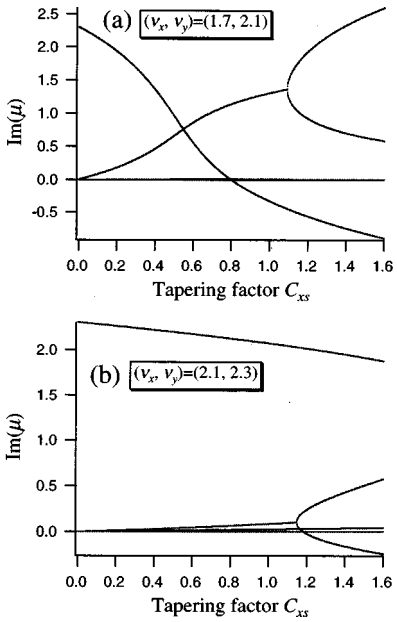

FIG. 1. Cooling rates vs tapering factor C_{xs} in the case where $f_s=0.9$. We have assumed a 1 MeV $^{24}Mg^+$ beam stored in the storage ring TARN II. The main TARN II parameters are summarized in Table I. Two different sets of betatron tunes have been considered: (a) $\nu_x=1.7$ and $\nu_y=2.1$ and (b) $\nu_x=2.1$ and $\nu_y=2.3$. For case (a), $d_c=5.004$ m while, for case (b), $d_c=3.384$ m.

where $G\equiv\gamma_0 d_c f_s/4\rho_m$, and we have assumed that $d_c\approx d_q$ for simplicity. Interestingly, the cooling rates of all three directions depend linearly on the tapering factor C_{xs}. As is clearly seen from Fig. 2, these analytic formulas agree well with the exact solutions evaluated from the dispersion relation.

In order to achieve strong simultaneous cooling in all three dimensions, the machine needs to operate near trans-

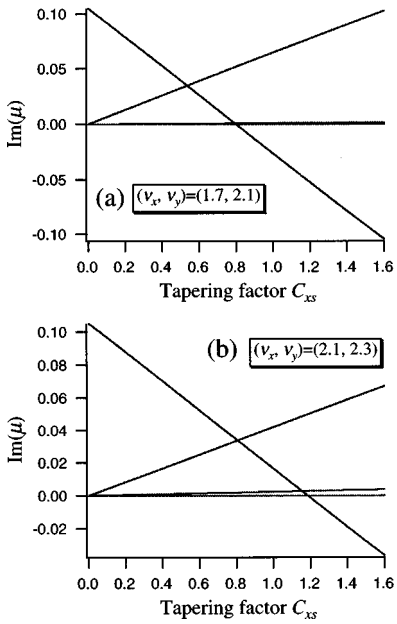

FIG. 2. Cooling rates vs tapering factor C_{xs} in the case where $f_s=0.1$. All parameters except for f_s are the same as those employed in Fig. 1.

verse coupling resonances where horizontal and vertical tunes are about equal, $\nu_x \approx \nu_y$ [8]. Provided that both betatron tunes are identical [24], we have, instead of Eq. (14),

$$\begin{aligned} &\mathrm{Im}(\mu) \approx G C_{\mathrm{xs}} \quad \text{(for the transverse motions)}, \\ &\mathrm{Im}(\mu) \approx f_s - 4 G C_{\mathrm{xs}} \quad \text{(for the longitudinal motion)}, \end{aligned} \tag{15}$$

where half of the horizontal cooling power has been given to the vertical direction. Equations (14) and (15) both indicate that the stable operating region is given by

$$C_{\mathrm{xs}} < \frac{\rho_m}{\gamma_0 d_c}, \tag{16}$$

which is independent of the cooling strength f_s. When the betatron tunes are adjusted to $(\nu_x, \nu_y) = (1.7, 2.1)$ in TARN II, the dispersion in the cooling section becomes 5.004 m, which gives the limiting tapering factor of 0.801 according to Eq. (16). In the case where $(\nu_x, \nu_y) = (2.1, 2.3)$, we find $d_c = 3.384$ m and, then, the threshold value of C_{xs} is 1.185. Obviously, these predictions are in good agreement again with the numerical results displayed in both figures.

IV. OPTIMIZATION OF THE TAPERING FACTOR

In this section, we determine the optimum tapering factor both for achieving the maximum cooling rates at high temperature and for achieving a crystalline structure at low temperature. For tapered electron cooling, the tapering factor may be controlled by varying the dispersion of the electron beam. For tapered laser cooling, the tapering factor may be changed by effectively adjusting the diffraction index of the prism.

A. Optimum tapering for cooling at high temperature

At high temperature, the optimum tapering factor for simultaneously achieving the maximum cooling rates in various directions can be obtained, in an ideal resonant situation, from Eq. (15) as $C_{\mathrm{xs}} = f_s / 5G$. Physically, cooling in the transverse directions comes from the change of betatron oscillation amplitude upon the change of particle momentum as well as the particle closed orbit at the cooling location. When the change of momentum varies linearly with the radial position and thus depends on the betatron phase, the difference in the amount of increase and decrease of the betatron amplitude at opposite betatron phase results in a net amplitude reduction [25].

B. Optimum tapering for beam crystallization

As the beam approaches the ultracold state, the optimum tapering factor for crystallization is determined by requiring all the particles to circulate with the same revolution frequency (or average angular velocity). In order for a crystalline beam to maintain its ordered structure, a radially outer particle has to traverse at an average velocity faster than that of an inner particle. Figure 3 shows the phase-space profile of a typical 3D crystal. We clearly observe the linear dependence of the longitudinal momentum on the horizontal coordinate. This observation also suggests that a too strong, *untapered* cooling force may destroy multidimensional crystalline structures since it tries to equalize the longitudinal velocities of all particles.

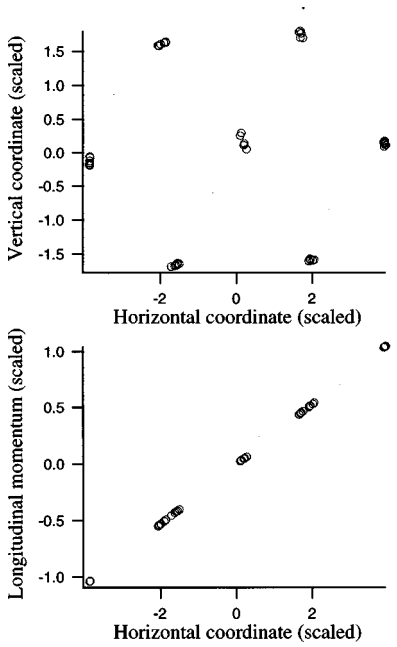

FIG. 3. Real-space and phase-space configurations of a single-shell crystalline beam. The lattice parameters of the storage ring TARN II [23] have been considered in this molecular dynamics simulation. The stored ions are 1 MeV $^{24}Mg^{+}$, and the betatron tunes have been adjusted to $\nu_x = \nu_y = 1.7$.

It is straightforward to estimate the optimum value of C_{xs}. First, note that the revolution time of a test particle with the velocity βc can be given by

$$T = \frac{1}{\langle \beta \rangle c} \int_0^{2\pi R} ds \sqrt{\left(\frac{dx}{ds}\right)^2 + \left(1 + \frac{x}{\rho}\right)^2}, \tag{17}$$

where $\langle A \rangle$ stands for taking the average of the quantity A over one turn, and the particle is assumed to move on the horizontal plane. On the other hand, at the final equilibrium state reached by the tapered cooling, $\Delta(\delta p/p)$ in Eq. (1) would vanish leading to $\delta p/p = \gamma C_{\mathrm{xs}} x / \rho_m$, which is equivalent to

$$\frac{\beta - \beta_0}{\beta_0} \approx C_{\mathrm{xs}} \frac{x}{\gamma_0 \rho_m}. \tag{18}$$

Requiring T to be equal to the design revolution time $2\pi R / \beta_0 c$, Eq. (17) together with Eq. (18) yield

$$\Delta L \approx \frac{2\pi R}{\gamma_0 \rho_m} \langle C_{\mathrm{xs}} x \rangle, \tag{19}$$

where ΔL is the path-length difference defined by

$$\Delta L = \int_0^{2\pi R} ds \sqrt{\left(\frac{dx}{ds}\right)^2 + \left(1 + \frac{x}{\rho}\right)^2} - 2\pi R. \tag{20}$$

Recalling that $|x/\rho| \ll 1$ and $|dx/ds| \ll 1$, the integral in Eq. (20) takes a finite value, in the first-order approximation, only within bending regions. Assuming that $x \approx \langle x \rangle$ in dipole

magnets of bending radius ρ_m, we obtain, from Eqs. (19) and (20), the average optimum tapering factor

$$\overline{C}_{\rm xs} \equiv \frac{\langle C_{\rm xs} x \rangle}{\langle x \rangle} \approx \frac{\gamma_0 \rho_m}{R}. \tag{21}$$

In order to determine more precisely the optimum tapering factor at the exact location of the cooling device, we need to consider the s dependence of $C_{\rm xs}$. Of course, the exact value of the optimum $C_{\rm xs}$ can be numerically evaluated from the relation between x and $\delta p/p$ in the ground-state crystalline structure (Fig. 3) obtained by MD simulation. Alternatively, we present, in the following, its analytical expression based on a mean-field potential model.

We first investigate the theoretical basis as to how the revolution frequencies of all stored particles become identical in a ground state. Noting that the physical-space density of a crystalline beam is roughly uniform, the mean space-charge potential is dominated by the linear force terms. In other words, we may approximately retain only the quadratic terms in the potential ϕ. Assuming that the cross section of the beam is elliptical as $(x/a)^2+(y/b)^2=1$, we can solve Poisson's equation to find

$$\phi = -\frac{qN}{2\pi\varepsilon_0}\left[\frac{x^2}{a(a+b)}+\frac{y^2}{b(a+b)}\right], \tag{22}$$

where a and b are s-dependent functions that have the same periodicity of the lattice structure, and N is the number of particles per unit length. To analytically determine the beam-size functions, we take the model

$$a''+K_x a-\frac{\varepsilon_x^2}{a^3}=\frac{2K_{\rm sc}}{a+b}, \quad b''+K_y b-\frac{\varepsilon_y^2}{b^3}=\frac{2K_{\rm sc}}{b+a}, \tag{23}$$

where $\varepsilon_{x,y}$ are related to the average beam dimensions $\sigma_{x,y}$ by $\varepsilon_{x,y}=\langle \sigma_{x,y}^2/\xi_{x,y}\rangle$, with $\xi_{x,y}$ as the transverse amplitude functions, and $K_{\rm sc}\equiv 2Nr_p/\beta_0^2\gamma_0^3$ with r_p as the classical radius of the particle. Notice that Eq. (23) is identical to the envelope equation familiar in the standard theory for linear transport systems [26]. We can prove that, in spite of the existence of momentum dispersion due to bending fields, the dynamical system treated here is perfectly self-consistent as long as the beam possesses a uniform density profile in real space [27]. The validity of the present model will be checked out in Sec. V by comparing the theoretical predictions with MD simulation results [28].

The use of Eq. (22) reduces the Hamiltonian in Eq. (7) to the simple form

$$\tilde{H}=\frac{1}{2}\left(\frac{1}{\gamma_0^2}-\frac{D_x}{\rho}\right)\frac{W^2}{(\beta_0 c)^2}+\frac{\tilde{p}_x^2+\tilde{p}_y^2}{2}+\frac{1}{2}\left[K_x-\frac{2K_{\rm sc}}{a(a+b)}\right]\tilde{x}^2 +\frac{1}{2}\left[K_y-\frac{2K_{\rm sc}}{b(a+b)}\right]\tilde{y}^2, \tag{24}$$

where we have, from Eqs. (8) and (9),

$$D_x''+\left[K_x-\frac{2K_{\rm sc}}{a(a+b)}\right]D_x=\frac{1}{\rho}, \tag{25}$$

indicating that the momentum dispersion D_x can be strongly detuned by the space-charge force. The longitudinal canonical equation of motion suggests that the usual definition of the phase slip factor $\eta=\alpha_{\rm sc}-1/\gamma_0^2$ [22], where the momentum compaction factor $\alpha_{\rm sc}=(2\pi R)^{-1}\oint ds(D_x/\rho)$ is linearly dependent on the dispersion D_x, still applies to the case of cold beams. As the beam approaches the ground state of crystallization, $\alpha_{\rm sc}$ changes considerably to naturally accomplish the isochronous condition $\eta=0$ such that the revolution frequencies of all stored particles are identical.

Apparently, betatron motion has been completely suppressed in ground states, which means that the coordinate $\tilde{x}$ is very close to zero. Recalling that $x=\tilde{x}-D_x W/\beta_0 c$, the transverse trajectory mainly originates from the dispersion function, i.e., $x\approx -D_x W/\beta_0 c$. Substitution of this formula into Eq. (18) leads to $(\beta-\beta_0)c\approx -WC_{\rm xs}D_x/\gamma_0\rho_m$. This equation can be rewritten as

$$C_{\rm xs}\approx \frac{\rho_m}{\gamma_0 D_x}. \tag{26}$$

Thus, to obtain the optimum tapering factor along the reference orbit, we only need to insert the dispersion function D_x, solved from Eqs. (23) and (25), into Eq. (26).

We readily notice, from the isochronous condition, that the average dispersion in a ground state is roughly equal to R/γ_0^2. Therefore, by taking the average of Eq. (26) over one turn, we obtain $\langle C_{\rm xs}\rangle \approx \gamma_0\rho_m/R$, which is consistent with Eq. (21). Equation (26) also gives us a simple interpretation of the limiting tapering factor discussed in Sec. III B. For an initial hot beam, the dispersion in the cooling section is d_c. On the other hand, the tapered cooling force pushes off-momentum particles onto particular closed orbits determined by the space-charge-detuned dispersion function D_x in Eq. (25). To prevent an input beam from average momentum increase after the interaction with a tapered laser, d_c must be less than the ground-state value of D_x, i.e., $D_x>d_c$ in Eq. (26), which yields the same condition as Eq. (16). Note that this argument again does not depend on the cooling strength f_s. In fact, Fig. 1 illustrates that Eq. (16) holds even for a large f_s.

V. MOLECULAR DYNAMICS RESULTS

We have performed molecular dynamics studies of space-charge-dominated and crystalline beams to confirm and generalize our findings presented in the earlier sections. In these studies, we numerically iterate the equations of motion, incorporating the characteristics of actual storage rings like bending and straight sections, and AG focusing. An Ewald-type [29] summation is performed in the azimuthal direction to evaluate the long-ranged Coulomb forces among particles and their image charges modeled in periodic ''supercells'' for computing efficiency.

We again choose the TARN II parameters summarized in Table I as an example to provide specific numerical results. The cooler ring ''TARN II,'' whose circumference is about 77.7 m, has the superperiodicity of 6 and contains four bend-

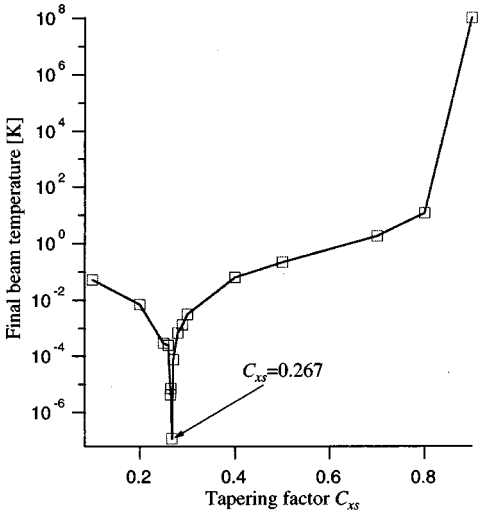

FIG. 4. Typical dependence of the equilibrium beam temperature on the tapering factor. The result was obtained with a MD code, assuming a 1 MeV $^{24}Mg^{+}$ beam stored in TARN II. The total number of the stored ions is $N_{\mathrm{tot}}=3.38\times10^{6}$. Here, $\nu_x=1.68$ and $\nu_y=1.85$, and we have installed two skew quadrupoles in each lattice period, whose integral strength per lattice period is 0.02 m^{-1} corresponding to the coupling factor $\Gamma_q\approx0.247$. The optimum tapering factor found in this simulation is 0.267 at which the beam has been completely crystallized.

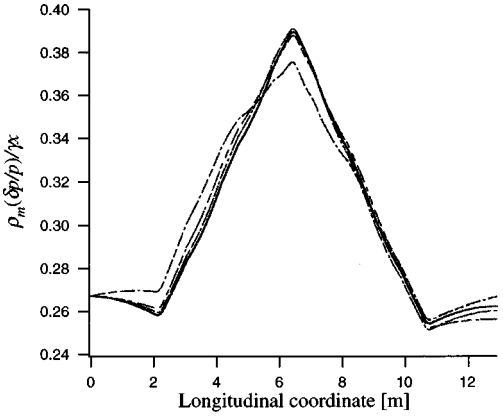

FIG. 5. Variation of the function $\rho_m(\delta p/p)/\gamma x$ along the reference orbit. $\rho_m(\delta p/p)/\gamma x$ of ten particles, calculated from a MD result, have been plotted. We have taken into account the same TARN II parameters as used in Fig. 4, and set $C_{\mathrm{xs}}=0.267$.

ing magnets in each lattice period. The orbit curvature in the bending regions is 4.01 m. Since the operating betatron tune is usually set at around 2 or even less, this ring is crystal friendly [30].

A typical C_{xs} dependence of final beam temperature [31] in TARN II is displayed in Fig. 4. We observe a sharp drop of temperature at $C_{\mathrm{xs}}\approx0.267$ where the beam has been fully crystallized to a 3D structure. For the tapering stability limit, we notice that the beam would heat up when C_{xs} exceeds around 0.9, in agreement with the mean-field prediction of Eq. (16), which gives a stability border of 0.98. For the optimum tapering gradient, the estimate of $C_{\mathrm{xs}}\approx0.324$ from Eq. (21), corresponding to the averaged C_{xs} over the ring, is again in reasonable agreement with the MD result that $C_{\mathrm{xs}}\approx0.267$.

We further compare the optimum tapering C_{xs} between the MD results and the mean-field prediction, Eq. (26), studying the s dependence of C_{xs} along the ring circumference. Figure 5 shows the results from the MD simulation, illustrating the longitudinal variation of $\rho_m(\delta p/p)/\gamma x$ of ten arbitrarily picked particles within one lattice period. Apart from small thermal noises, all particles have an identical $\rho_m(\delta p/p)/\gamma x$, which represents the optimum tapering factor. In this simulation, the cooling section is located at both ends of the picture, where the quantity $\rho_m(\delta p/p)/\gamma x=0.267$ is consistent with the optimum C_{xs}.

The task now is to examine whether the mean-field theory can reproduce the same result as Fig. 5. For convenience, we rewrite Eqs. (23) as

$$\tilde{a}''+K_x\tilde{a}-\frac{\tilde{\epsilon}_x^2}{\tilde{a}^3}=\frac{2}{\tilde{a}+\tilde{b}},\quad \tilde{b}''+K_y\tilde{b}-\frac{\tilde{\epsilon}_y^2}{\tilde{b}^3}=\frac{2}{\tilde{b}+\tilde{a}},\tag{27}$$

where $\tilde{a}=a/\sqrt{K_{\mathrm{sc}}}$, $\tilde{b}=b/\sqrt{K_{\mathrm{sc}}}$, $\tilde{\epsilon}_x=\epsilon_x/K_{\mathrm{sc}}$, and $\tilde{\epsilon}_y=\epsilon_y/K_{\mathrm{sc}}$. Similarly, the parameter K_{sc} is eliminated from Eq. (25) as

$$D_x''+\left[K_x-\frac{2}{\tilde{a}(\tilde{a}+\tilde{b})}\right]D_x=\frac{1}{\rho}.\tag{28}$$

For the TARN II example considered in this section, we may set $\tilde{\epsilon}_x\approx\tilde{\epsilon}_y(\equiv\tilde{\epsilon})$ since the betatron tunes are close to each

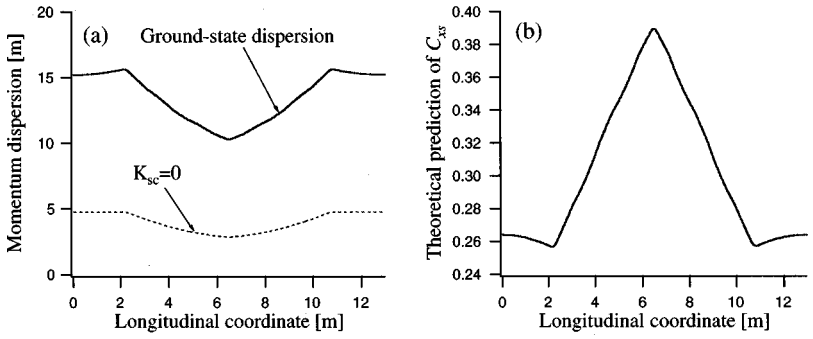

FIG. 6. Theoretical predictions: (a) The solid line corresponds to the momentum dispersion in a ground state while the dotted line corresponds to that in the absence of space charge, i.e., the case of $K_{\mathrm{sc}}=0$; (b) the optimum tapering factor along the reference orbit, predicted by Eq. (26).

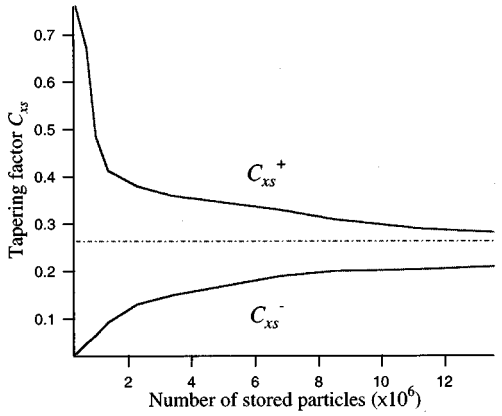

FIG. 7. Acceptable range of tapering factor; $C_{\rm xs}^{+}$ and $C_{\rm xs}^{-}$ represent, respectively, the upper and lower limit of $C_{\rm xs}$ required for beam crystallization. The dot-dash line indicates the ideal value predicted by the theory. Note that the transition from 1D to 3D crystalline structure takes place when the number of stored particles is around 1.2×10^6 in the present example.

other. To choose a proper value of $\tilde{\epsilon}$ in Eq. (27), the isochronous condition $\eta=0$ is employed. By numerically finding periodic solutions to Eqs. (27) and (28), we conclude that $\tilde{\epsilon}$ must be about 5.4 in the present case for the slip factor η to be zero. The dispersion function obtained through this numerical procedure has been plotted in Fig. 6(a). Obviously, the effect of space-charge detuning on momentum dispersion is significant for a beam at crystalline-state density. The function D_x shown in Fig. 6(a) is further substituted into Eq. (26) to generate Fig. 6(b), which is in excellent agreement with the MD results in Fig. 5. This inversely indicates that the envelope model introduced in Eq. (23) is valid for our discussion, and that the isochronous condition is certainly realized in the ground states. Furthermore, we have shown that ground-state dispersion can uniquely be determined once the lattice structure of a storage ring is fixed.

Finally, it is of practical interest to evaluate the acceptable range of error in $C_{\rm xs}$ for achieving beam crystallization. The definition of the threshold temperature is, however, quite arbitrary because no sharp phase transition has so far been encountered in coasting beams [32]. Therefore, we simply define here a crystal temperature of 0.02 K [33, Fig. 8], below which the beam is considered crystallized. Figure 7 shows the upper and lower limit of the acceptable tapering factor according to this definition. It is evident that the acceptable range becomes particularly large for one-dimensional (1D) crystals. We have further verified, based on systematic MD simulations, that this range is insensitive

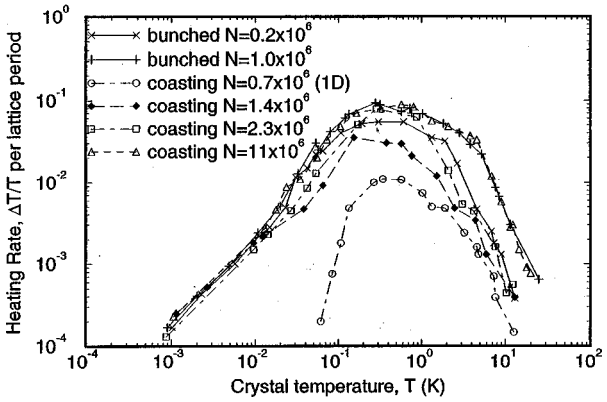

FIG. 8. Heating rate curves for bunched and coasting beams at different line densities.

to the value of f_s when f_s is greater than about 0.3, and is also insensitive to whether the beam is azimuthally bunched.

VI. SUMMARY

To conclude, we have given a satisfactory theoretical description of the tapered beam cooling. It has been demonstrated that this cooling scheme provides both transverse-longitudinal coupling essential for 3D beam cooling, and a promising method for achieving the crystalline beams in a storage ring. The linear cooling rates have been evaluated from a characteristic equation. A mean-field Hamiltonian has also been established to understand some important features of crystalline beams. In particular, we have shown how, when the necessary conditions for beam crystallization are satisfied, the revolution frequencies of all particles are detuned by the space-charge force to converge on the same value in a ground state. The space-charge-detuned dispersion function and the isochronous condition have been employed to predict the optimum value of the tapering factor at any arbitrary location along the design orbit. It has been found that analytical predictions from the mean-field model are in excellent agreement with the results from the molecular dynamics calculations.

ACKNOWLEDGMENTS

The authors would like to thank Dr. X.-P. Li for originally developing the MD simulation program. They would also like to express their sincere gratitude to Dr. A. M. Sessler for his stimulating suggestions in the course of this work. One of the authors (H.O.) is indebted to Professor S. Y. Lee for valuable discussions on space-charge-dominated beam dynamics.

[1] V. V. Parkhomchuk and N. S. Dikansky, Sov. J. Tech. Phys. **50**, 1411 (1980); E. E. Dement'ev, N. S. Dikansky, A. S. Medvenko, V. V. Parkhomchuk, and D. V. Pestrikov, Zh. Tekh. Fiz. **50**, 1717 (1980).

[2] A. Rahman and J. P. Schiffer, Phys. Rev. Lett. **57**, 1133 (1986); R. W. Hasse and J. P. Schiffer, Ann. Phys. (NY) **203**, 419 (1990); J. P. Schiffer, Phys. Rev. Lett. **70**, 818 (1993).

[3] J. Wei, X.-P. Li, and A. M. Sessler, Brookhaven National Laboratory Report No. BNL-52381, 1993; J. Wei, X.-P. Li, and A. M. Sessler, Phys. Rev. Lett. **73**, 3089 (1994).

[4] D. J. Wineland and H. Dehmelt, Bull. Am. Phys. Soc. **20**, 637 (1975); T. Hänsch and A. Schawlow, Opt. Commun. **13**, 68 (1975).

[5] S. Schröder, R. Klein, N. Boos, M. Gerhard, R. Grieser, G. Huber, A. Karafillidis, M. Kieg, N. Schmidt, T. Kühl, R. Neumann, V. Balykin, M. Grieser, D. Habs, E. Jaeschke, D.

Krämer, M. Kristensen, M. Music, W. Petrich, D. Schwalm, P. Sigray, M. Steck, B. Wanner, and A. Wolf, Phys. Rev. Lett. **64**, 2901 (1990).

[6] J. S. Hangst, M. Kristensen, J. S. Nielsen, O. Poulsen, J. P. Schiffer, and P. Shi, Phys. Rev. Lett. **67**, 1238 (1991).

[7] H-J. Miesner, R. Grimm, M. Grieser, D. Habs, D. Schwalm, B. Wanner, and A. Wolf, Phys. Rev. Lett. **77**, 623 (1996).

[8] H. Okamoto, Phys. Rev. E **50**, 4982 (1994).

[9] H. Okamoto, A. M. Sessler, and D. Möhl, Phys. Rev. Lett. **72**, 3977 (1994).

[10] T. Kihara, H. Okamoto, Y. Iwashita, K. Oide, G. Lamanna, and J. Wei (unpublished).

[11] To form and maintain a crystalline beam, the storage-ring lattice must satisfy the following two conditions: (a) the beam energy is smaller than the transition energy of the ring and (b) the lattice superperiodicity divided by $2\sqrt{2}$ is greater than both betatron tunes. See, e.g., J. Wei, X.-P. Li, and A. M. Sessler, in *Advanced Accelerator Concepts*, Proceedings of the Sixth Advanced Accelerator Concepts Workshop, Fontana, 1994, AIP Conf. Proc. 335, edited by P. Schoessow (AIP, New York, 1995).

[12] J. Wei, A. Draeseke, A. M. Sessler, and X.-P. Li, *Crystalline Beams and Related Issues* (World Scientific, Singapore, 1996), p. 229.

[13] J. P. Schiffer, *Crystalline Beams and Related Issues* (Ref. [12]), p. 217.

[14] J. Wei, H. Okamoto, and A. M. Sessler, Phys. Rev. Lett. **80**, 2606 (1998).

[15] This equation is equivalent to Eq. (4) in Ref. [14].

[16] Ya. Debenev (private communication).

[17] S. Y. Lee and H. Okamoto, Phys. Rev. Lett. **80**, 5133 (1998).

[18] Except for Sec. V and Fig. 8 where the MD study shows a similar behavior of crystal heating and tapered cooling.

[19] In the tapered cooling scheme, the installation of skew quadrupole magnets is usually required to couple the vertical motion to the horizontal motion. However, as we will see later, the general properties of tapered cooling can be well described by the present Hamiltonian unless the skew field is too strong.

[20] T. Suzuki, Part. Accel. **12**, 237 (1982).

[21] In general, the space-charge potential contains the linear cross term that gives rise to vertical dispersive effects. In such a case, it is convenient to define the vertical dispersion function by introducing the generalized Suzuki function (See Ref. [17]). For crystalline beams, however, the vertical dispersion is mostly negligible due to the symmetry of the configuration.

[22] For more information on the notions of the transfer matrices and momentum compaction factor, etc., see, e.g., H. Wiedemann, *Particle Accelerator Physics* (Springer-Verlag, Berlin, 1993).

[23] T. Katayama *et al.* (unpublished).

[24] Provided that a linear coupling potential like that of a skew quadrupole is present, it is, in principle, impossible to *exactly* equalize the betatron tunes. The possible minimum difference between them is proportional to the strength of the coupling field Γ_q.

[25] With conventional untapered cooling, the change in momentum is constant across the radial displacement. The net change of betatron amplitude is zero with the averaging over betatron phase.

[26] See, e.g., M. Reiser, *Theory and Design of Charged Particle Beams* (John Wiley & Sons, Inc., New York, 1994).

[27] The phase-space-distribution generating a uniform density in real space is referred to as the Kapchinskij-Vladimirskij (KV) distribution. We must, however, keep in mind that the phase-space configuration of a crystalline beam is essentially different from that of a KV beam, even if the real-space density profiles look similar to each other in an average sense. The present approach is thus not applicable to the purpose of constructing a *fine-grained* picture of ground states. For the details of the KV distribution function, see I. M. Kapchinskij and V. V. Vladimirskij, in *Proceedings of the International Conference on High Energy Accelerators* (CERN, Geneva, 1959), p. 274.

[28] It is also worthy to note that, as in self-consistently proven in Ref. [17], the condition of crystal maintenance is a natural consequence of Eq. (23).

[29] P. P. Ewald, Ann. Phys. (Leipzig) **64**, 253 (1921).

[30] At present, there exist only two storage rings in the world in which a laser cooling system has been installed, namely, the TSR ring [5] at MPI, Heidelberg, and the ASTRID ring [6] at Aarhus University, Denmark. However, neither of these storage rings satisfies the necessary condition of crystal maintenance. Thus, in order to give specific numerical results, we adopt the TARN II parameters as the example [23].

[31] The beam temperature for the crystalline beam study is defined to be proportional to the deviations of the normalized canonical momenta from their ground-state values, then squared and averaged over many lattice locations and periods, and over all the particles [14]. (The definitions of the normalized momenta have been given, e.g., in Ref. [12]). When the system temperature is sufficiently higher than the breakup temperature of the crystalline state, which in this case is about $T=1$ K, this temperature is the same as the conventionally used temperature T_B, given by the relation

$$[T_{Bx},T_{By},T_{Bz}]=\frac{\beta_0^2\gamma_0^2mc^2}{2k_B}\left[\frac{(\varepsilon_{\rm rms})_x}{\langle\beta_x\rangle},\frac{(\varepsilon_{\rm rms})_y}{\langle\beta_y\rangle},\frac{1}{\gamma_0^2}\left(\frac{\delta p}{p}\right)^2_{\rm rms}\right],$$

where k_B is the Boltzmann constant, $(\varepsilon_{\rm rms})_{x,y}$ are the unnormalized root-mean-squared (rms) beam emittance, $(\delta p/p)_{\rm rms}$ is the rms momentum spread, and $\langle\beta_{x,y}\rangle$ are the average betatron amplitude functions. However, when the beam is cooled longitudinally so that $\delta p/p$ and T_{Bz} both approach zero, the longitudinal crystal temperature can still be high since the z motion is coupled with the x motion through dispersion, and that transverse temperature is still high.

[32] The situation might be quite different for bunched beams since they are substantially three-dimensional.

[33] The corresponding normalized temperature is 0.05 [12]. The MD study shows that below this temperature strong ordering between particles occurs, and the crystal heating rate is low as shown in Fig. 8.